TURBULENT SCALAR MIXING IN COAXIAL JET FLOWS

Paulo C. Ferrão, Manuel V. Heitor, Mário F. de Matos and Renato K. Salles
Mechanical Engineering Department
Instituto Superior Técnico
Av. Rovisco Pais, 1049-001 Lisboa
Technical University of Lisbon
Portugal

ABSTRACT

The turbulent characteristics of the developing region of an axisymmetric coaxial jet of CO_2 (Re_i=15000) and air (Re_o=50000) are analysed making use of experimental results obtained in the initial region where most of the mixing takes place. Time-resolved velocity and scalar fields were characterised by laser Doppler velocimetry and laser Rayleigh scattering, while the instantaneous velocity field was analysed with double-exposure photographic particle image velocimetry. Linear imaging of laser Rayleigh scattering was used to acquire instantaneous information about the scalar field that enables the quantification of scalar dissipation. As a result, scalar dissipation distribution can be associated to the evolution of the Reynolds stresses along the jet and the later is related to the location of large-scale structures, which are identified with the locus of maximum vorticity.

1. INTRODUCTION

This paper is focused on the experimental analysis of turbulent scalar mixing in coaxial jet flows, as it constitutes a critical step to improve understanding of mixing in highly turbulent reacting flows. Variable density effects are a consequence of heat release due to reaction, which have shown to alter turbulent mixing in flames (Starner and Bilger, 1986; Heitor et al., 1987; Ferrão and Heitor, 1998).

In this context, the present contribution consist on the analysis of a comparatively simple flow in the form of two co-flowing jets of different gases, allowing for the characterisation of the mixing processes in variable density jets, precluding the inherent complexities of chemical reaction. The primary interest is focused in the developing region of the coaxial jet, where most of the mixing takes place.

Axisymmetric coaxial turbulent jets at various velocity ratios have been widely studied, but most of the research has been limited to time-averaged velocity and turbulence quantities and spectra in constant density flows. The majority of the studies carried out in the last decades conclude about a faster development in coaxial jets when compared to single jets. In particular, the occurrence of vortex shedding and flow instabilities in the wake of the inner pipe was identified by Ribeiro and Whitelaw (1980) to be responsible by several features of coaxial jet flows that cannot be represented by conventional turbulent mechanisms. Kwan and Ko (1977) attempt to infer the near-field vortex structure of subsonic coaxial jets based on pressure and velocity measurements, suggesting that the developing structures in this region could be considered physically similar to those in single jets. Lately, Dahm et al.(1992) have demonstrated that the structure of the vortex patterns which are formed in the near-field of coaxial jets differs from the combination of single jets.

In addition, as suggested by Pagé et al.(1998), variable-density effects contribute for the complexity of turbulent mixing and, as a consequence, additional experimental studies are required to improve the understanding of this phenomena. In particular, large-scale motions and its influence on vorticity distribution, Reynolds stresses and scalar dissipation have not been experimentally identified.

The present work provides experimental characterisation of large-scale structures and its effect on both the Reynolds stresses and on scalar dissipation, and is intended to improve understanding of these processes, which ultimately influence turbulent mixing in variable-density coaxial jets.

The following section describes the diagnostic techniques used. Experimental results are presented and briefly discussed in section 3 and the final section presents the main conclusions of the work.

2. EXPERIMENTAL METHOD

2.1. The Flow Studied

The experimental rig used throughout the work includes two concentric stainless steel ducts where CO_2 flows in the inner duct surrounded by an air jet. An external annular airflow at very low velocity (0.5m/s) provides accurate boundary conditions. As depicted in figure 1, the inner tube has an inside diameter, d=2mm, and 1211mm in length and is 1-mm-thick. The two air jets result from a primary annulus, D=24mm in diameter, and a secondary annulus of 150mm in diameter.

The rig was designed and built in order to obtain fully developed turbulent flows at the exit plane. The annuli formed by the innermost and the middle tube is equipped with 3 honeycomb structures, 50mm long in order to remove any swirl component of the flow.

The experimental rig is mounted on a three-dimensional traverse system, with a spatial resolution of 0.2mm in any direction.

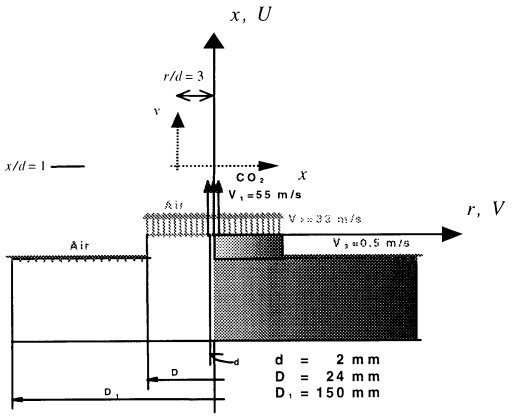

Figure 1. Geometry and boundary conditions for the flow studied (dashed co-ordinates were used for P.I.V. and linear measurements).

The density ratio of the inner jet to the outer coaxial jet is of 1.5, while the ratio of the bulk mean axial velocity in the coannular air jet to the central jet at the exit plane is 0.6. This is associated to an average velocity of 55m/s in the central jet and 33m/s in the outer jet, which correspond to a Reynolds number characteristic of the air jet based on the equivalent diameter (D-d) of Re=50000, and a Reynolds number characteristic of the CO_2 jet and based on the inner diameter, of 15000.

The CO_2 is supplied to the inner jet from a 99.5% pure gas pressurised cylinder, while the air is supplied from a fan and is filtered by means of a 1μm particle filter. Both the CO_2 and air pressure is controlled to maintain constant flow rates, which are monitored by individual flowmeters.

2.2. L.D.V. Measurements

The instrumentation used throughout this work for the velocity time-resolved measurements is based on a single laser light source (5W multiline argon-ion laser).

The laser Doppler velocimeter is based on the green light (514.5nm) of the laser and was operated in dual-beam, forward-scatter mode with sensitivity to the flow direction provided by a rotating diffraction grating. The calculated dimensions of the measuring volume at the e^{-2} intensity locations were 606μm in length and 44μm in diameter. The flow was seeded with 1μm-diameter aluminium oxide particles, Al_2O_3, which are introduced by a set of cyclones. The main features of this velocimeter were outlined by Ferrão and Heitor (1998).

2.3. P.I.V. Measurements

Double-exposure photographic particle image velocimetry was used together with a spatial autocorrelation technique for whole field velocity measurements.

The coaxial jet was illuminated by a Q-switched double-pulsed Nd:YAG laser (Spectra Physics Pulsed Nd:YAG laser GCR-130) with an output energy of approximately 0.2J per pulse. The 6mm diameter laser beam was expanded in a divergent cylindrical lens and collimated in a plan-convex lens ($f^{\#}7$) that focuses the beam in the test section, giving rise to a light sheet, 145mm in height and 0.2mm minimum thickness.

The flow was seeded with 1μm diameter Al_2O_3 particles, which allow for accurate photographic recording of particle images. The seeding concentration was approximately 25 to 30 particles/mm^3, in both the inner CO_2 jet and in the outer air jet.

The coaxial jet flow field was photographed using a 60×70mm^2 view camera, making use of a macro M140mm high quality lens, using an aperture of $f^{\#}16$ at unit image magnification in order to minimise lens aberrations.

Details of the experimental facility and data processing are available in Caldas et al.(1998).

2.4. Rayleigh Scattering Diagnostics

2.4.1. Point Measurements. The single-point laser Rayleigh scattering system is derived from that described by Ferrão and Heitor (1998), where the main data acquisition system was changed by a 16 bits analogue-digital converter.

The system operates from the blue line (488nm) of the same laser source that was used for the time-resolved velocity measurements. The beam is expanded (5:1) and then focused to overlap the control volume of the L.D.V. system. The light is converged in a beam waist of 50μm diameter was collected at 90° from the laser beam direction using a collection optics characterised by a magnification of 1, and passed through a 1mm-length slit. A 1nm-bandwidth interference filter and a polariser filter were

used to optimise the signal-to-noise ratio. The signal was amplified and low pass filtered at 10kHz before digitalisation. The temporal resolution of the system depends on the integration time associated with this filter, which is quantified to be 50μs.

2.4.2. Linear measurements. The instrumentation used to measure the scalar dissipation rate is based on the collection of the light scattered from Nd:YAG pulsed laser beams (9ns) using a cooled linear array CCD camera. The 532nm-wavelength laser beam is converged in a beam waist of 50μm diameter by an one-meter focal length lens. The light scattered was collected at 90° from the laser beam direction with a magnification of 1.5 and detected by the CCD array. A large number of measurements were made along (about 600 in each measurement station), and the image was analysed by dedicated software, which validated the results depending on the presence of particles.

The individual instantaneous scalar dissipation measurements were averaged and an error analysis has shown that, for a confidence interval of 95%, the overall uncertainty in scalar dissipation is under 15%.

3. ANALYSIS OF THE EXPERIMENTAL RESULTS

The main features of the jet studied are presented in figure 2, which shows centreline distributions of the reciprocal of the mean axial velocity and the Reynolds normal stresses (axial and radial components) for the results obtained and for previous results from Ribeiro and Whitelaw (1980) obtained in uniform density coaxial jets.

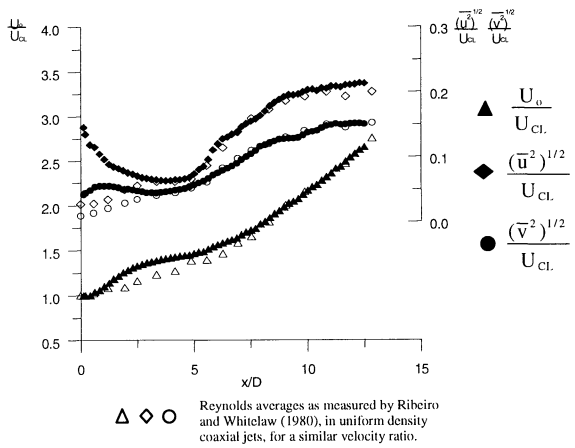

Figure 2. Centreline distributions of Favre-averaged velocity, axial and radial turbulence intensities.

The evolutions represented show that although the annular flow does not influence the mean axial velocity at the centreline up to $x/D \approx 1$, it does affect the Reynolds stresses. Between one and two diameters downstream the jet tip, the mean velocity along the centreline decays rapidly. This region is followed by a region that extends up to five diameters, where the mean and turbulent components of the axial velocity are approximately constant and the turbulent velocity is comparatively low. Downstream $x/D=5$, mean axial velocity tends asymptotically to a value which is inversely proportional to the distance from the nozzle tip and, particularly between $x/D=5$ and $x/D=7$, the axial normal stress increases significantly.

The mean velocity profile appears to be self-preserving downstream $x/D=7$. However, turbulence intensity, $\overline{u}^2$ and $\overline{v}^2$, do only achieve self-similarity characteristics downstream of $x/D=12$, which is to say that the behaviour of the mean flow and of the Reynolds stresses is no longer dependent on the initial conditions.

The flow characteristics downstream $x/D=4$ are typical of coaxial uniform density turbulent jets, in that the mean and turbulent flows downstream of the jet duct tend to self-similarity, and in particular, the present results are consistent with those of Ribeiro and Whitelaw (1980). The near tip zone is influenced by variable density effects as the evolutions presented in figure 2 were not found in previous studies on uniform density flows available in literature.

The time-averaged velocity field characterisation of the initial region of the jet is presented in figures 3 and 4, which show radial distributions of mean axial and turbulent characteristics. The central jet is clearly identified upstream $x/D=3.33$ and this can be confirmed in terms of time-averaged scalar mixture fraction as represented in figure 5.

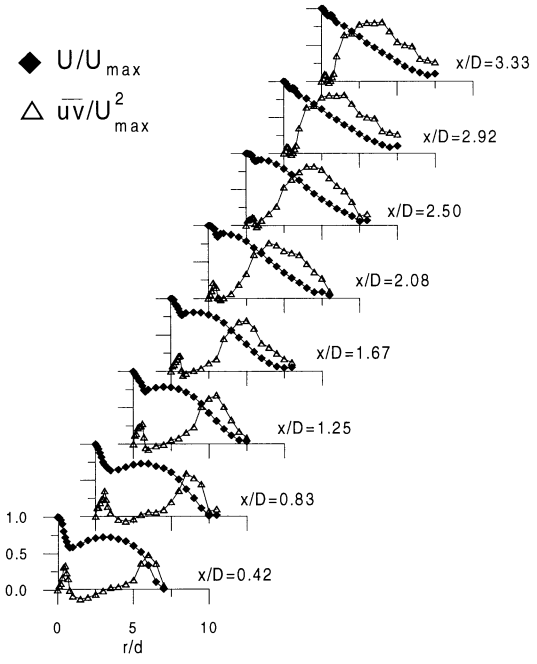

Figure 3. Radial distributions of mean axial velocity and Reynolds shear stresses.

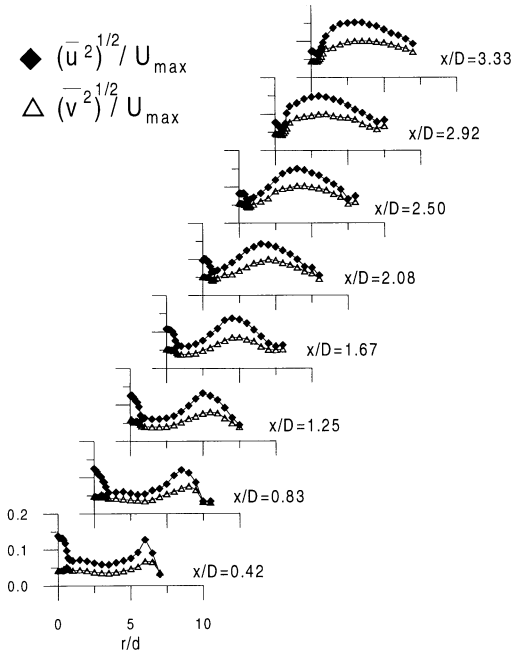

Figure 4. Radial distributions of axial and radial turbulence intensities.

Turbulent diffusion along the flow is associated to the evolution of the Reynolds stresses, which identifies zones of outward turbulent transport of axial momentum, characterised by $\overline{uv}$ >0, namely in the inner jet and in the outer shear layer. An intermediate zone of inward turbulent transport of axial momentum, where $\overline{uv}$ <0 was also identified. The locations where $\overline{uv}$ cross the abscissa are in qualitative agreement with the occurrence of the maxima and minimum in the mean velocity profiles, or the shear stress is zero at locations of zero mean axial velocity gradient, as predicted by eddy viscosity models.

Downstream the axial station at *x/D*=2.92 the inner peak of the Reynolds shear stress radial profiles vanishes, which suggests that turbulent mixing has reached the centreline. The present results also show that the axial and radial normal stresses exhibit a double peak in the region where the inner jet is identified, and therefore, the radial derivative of the axial normal stress can also contribute significantly for axial momentum diffusion.

The evolution of mixture fraction $\xi=M_{CO2}/(M_{air}+M_{CO2})$ can be used to characterise the scalar field and to quantify the process of diffusion of CO_2 in this flow, as represented in figure 5. The considerations established for the velocity field can be extended to the scalar characteristics of figure 5 in that the radial distributions of the scalar mixture fraction fluctuations exhibit a local minimum at the centreline and a peak at the maximum radial gradient of mean CO_2 concentration.

The radial distribution of scalar mixture fraction can be well fitted by a gaussian curve when divided by the mixture fraction characteristic of the centreline at each axial location, as demonstrated in figure 6a. The radial co-ordinate was non-dimensionalised by the axial location $\eta_{1/2}=r/(x-x_0)$. Here x_0 is the virtual origin of the jet computed as the location where the linear regression of the radial locations where $\xi=1/2\xi_{CL}$, expressed as a function of the axial distance, crosses the abscissa. The calculated value for the virtual origin was 32mm upstream the jet tip. The evolution of figure 6a can be mathematically described by the function $\overline{\xi}/\overline{\xi}_{CL} = exp\left(-1253.2\eta_{1/2}^2\right)$. Figure 6b shows that downstream *x/D*=1.25 the mixture fraction fluctuations can also be modelled adopting a similar procedure, although the mean values tend to achieve self-similarity further upstream.

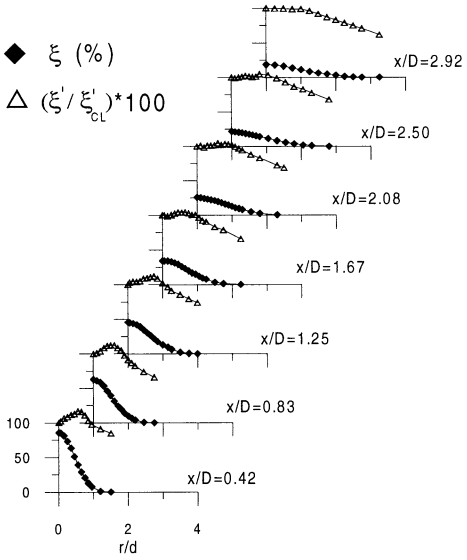

Figure 5. Radial distributions of time-averaged and turbulent mixture fraction.

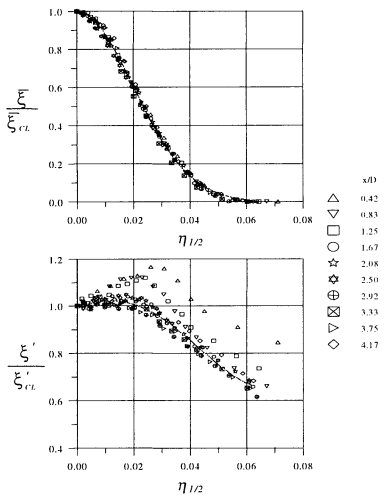

Figure 6. Normalised radial profiles of:
(a) Time-averaged mixture fraction;
(b) Turbulent mixture fraction.

The quantification of scalar dissipation, which is related to the square of the scalar mixture fraction gradient, constitutes an important step for turbulence modelling and, in particular, is related to flame stabilisation for reacting flows. Transversal evolutions of the mean transverse scalar dissipation (eq.1, where $\mathcal{D}$ is the binary diffusivity of CO_2 in air) for different axial locations is presented in figure 7 together with mean mixture fraction linear measurements.

$$\overline{\chi}_x = 2 \cdot \mathcal{D} \overline{\left(\frac{\partial \xi}{\partial x} \frac{\partial \xi}{\partial x} \right)} \qquad (1)$$

The ability of the instantaneous linear measurement technique to quantify the scalar field is demonstrated by the agreement of the values of $\overline{\xi}$ obtained, when compared to the point measurements presented in figure 5. Scalar dissipation field, $\chi(x,t)$, was computed using central differences on adjacent pixels of the instantaneous line measurements obtained.

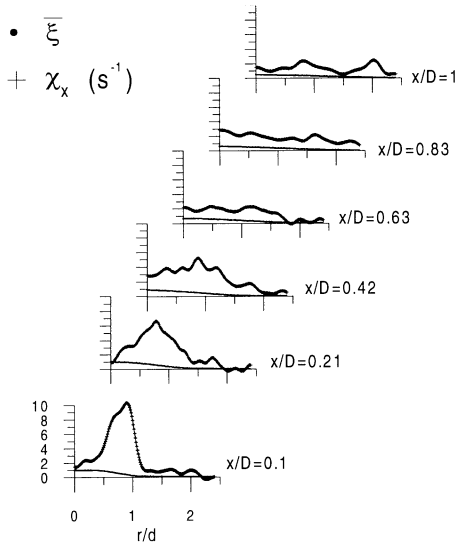

Figure 7. Mixture fraction and radial scalar dissipation rate profiles in the initial region of the jet.

As it is clearly illustrated in figure 7, the radial scalar dissipation is maxima in the initial region of the jet, near the jet tip up to x/D=0.5, between r/d=0.5 and r/d=1.5, which may be interpreted as the region of most intense mixing between the inner and the outer jet. This is associated with the stretching of the large-scale structures that were identified to be aligned with the mean flow in this particular region. In addition, this region coincides with the location of maximum vorticity values, as discussed in the next paragraphs.

The vorticity structure of the coaxial jet can be determined by the maps of the out-of-plane component of the vorticity, w_z, as measured in a vertical plane crossing the jet axis. The results obtained, and represented in figure 8b, have shown that $\partial u/\partial x$ is the main component to the final value of vorticity over the measured zone in the coaxial jet mixing layer. The largest values of the vorticity were observed in the inner-to-outer jet mixing layer on the initial merging zone, where large velocity gradients exist. The results show three zero-vorticity lines, namely along the centre of the jet and limiting two outer small vorticity zones of opposite sign. In its initial stage of development, the coaxial jet consists of two symmetrical inner mixing layers, which are limited by a core of irrotational flow in the annular jet of air.

Although the direct observation of the velocity maps as obtained by PIV measurements does not identify any coherent structure in the flow field, these structures can be visualised by subtracting an appropriate value to the velocity in each point of the vectorial map, as described in Caldas et al.(1998). The sample results of figure 8 quantify the propagation of coherent structures that occurs in the locus of maximum vorticity and correspond to the flow region where the Reynolds shear stresses are maxima.

4. CONCLUSIONS

The analysis above has characterised the turbulent structure of a coaxial jet flow, including the effect of large-scale motions on turbulent mixing. Single-point measurements were complemented with new information on the scalar dissipation rate, and the use of PIV has allowed for the identification of large-scale structures and the quantification of the vorticity field.

The evidence is that the positive local peaks in the distribution of shear stress for r/d≈1 correspond to an annular vortex structure, as defined in the vorticity map of figure 8. This annular vortex structure dominates turbulent mixing and is related with positive vorticity (counter-clockwise) on the left side of the flow represented in figure 8.

Figures 8a and 8c establishes the presence of large-scale structures that occur in the inner mixing layer of the jet studied due to shear instability in the wake of the inner pipe wall. These structures are seen to grown linearly in the plane of the measurements as they convect for downstream locations. During their growth, the corresponding intensity vorticity level decreases, as predicted by transport and diffusion vorticity theorems.

The structure in the inner mixing layer of the coaxial jet is affected by fluid from both the inner and the annular jet. As it is observed in figure 8 the inner region of the large-scale structures formed can be associated to the peak in the radial profiles of mixture fraction fluctuations shown on figure 5.

Upstream axial locations of x/D=0.5, radial profiles of scalar dissipation exhibit a distinctive peak, which vanishes rapidly prior to the measurement station at x/D=0.63. The attenuation of radial component of the scalar dissipation and the radial enlargement of its peak for downstream locations are consistent with the attenuation of vorticity and shear stress and with the growth of the turbulent structures identified by PIV measurements.

REFERENCES

Caldas, F., Ferrão, P., Heitor, M.V., and Matos, M.de, 1998, "On the Analysis of Turbulent Scalar Mixing in Coaxial Jet Flows," *9th Intl. Symp. on Applications of Laser Techniques to Fluid Mechanics*, Lisbon, July13-16, paper17.3.

Dahm, W.J.A., Frieler, C.E., and Tryggvason, G., 1992, "Vortex Structure and Dynamics in the Near Field of a Coaxial Jet," *J. Fluid Mech.*, Vol.241, pp.371-402.

Ferrão, P., and Heitor, M.V., 1998, "Probe and Optical Diagnostics for Scalar Measurements in Premixed Flames," *Experiments in Fluids*, 24, pp. 389-398.

Heitor, M.V., Taylor, A.M., and Whitelaw, J.H., 1987, "The Interaction of Turbulence and Pressure Gradients in Baffle-Stabilised Premixed Flames," *J. Fluid Mech.*, Vol.181, pp.387-413.

Kwan, A.S.H., and Ko, N.W., 1976, "The Initial Region of Subsonic Coaxial Jets. Part 2," *J. Fluid Mech.*, Vol.82, pp.273-287.

Pagé, J., Sarh, B., and Gokalp, I., 1998, "Experimental Determination of the Turbulent Kinetic Energy and the Dissipation Rate in Variable Density Turbulent Jets," *9th Intl. Symp. on Applications of Laser Techniques to Fluid Mechanics*, Lisbon, July13-16, paper17.2.

Ribeiro, M.M., and Whitelaw, J.H., 1980, "Coaxial Jets with and without Swirl," *J. Fluid Mech.*, Vol.96, pp.769-795.

Starner, S.H., and Bilger, R.W., 1986, "Joint Measurements of Velocity and Scalars in a Turbulent Diffusion Flame with Moderate Swirl," *21th Symp. (Intl.) on Combustion*, The Combustion Institute, pp.1569-1577.

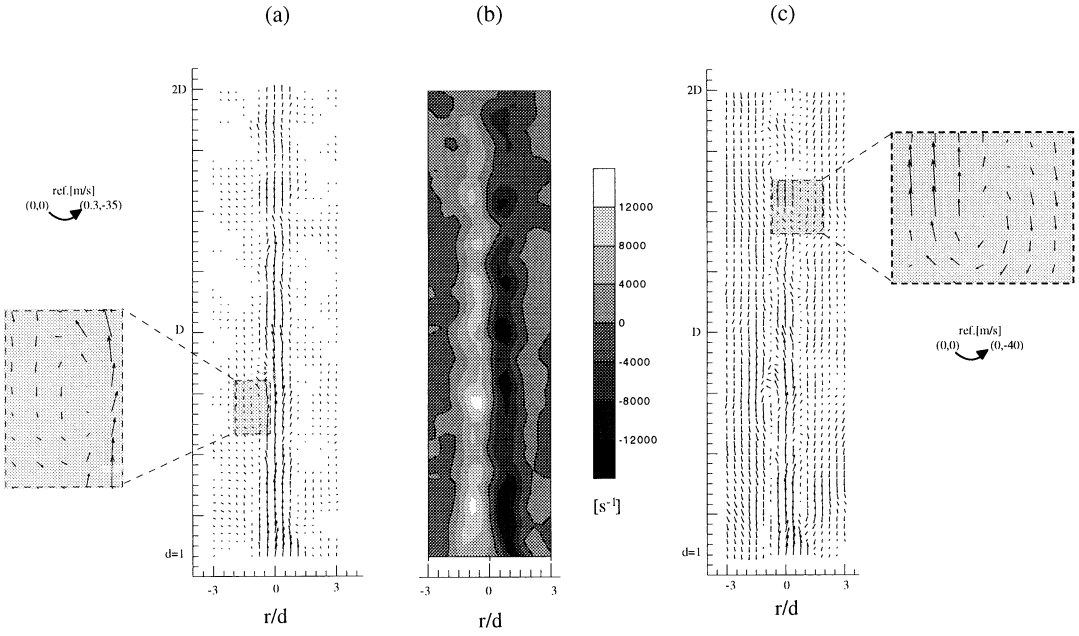

Figure 8. Sample PIV measurements in coaxial jet:
(a) Sample results in a frame of reference convecting at u(-0.3,35) m/s, with identification of large-scale motion around x=0.75D,
(b) Instantaneous vorticity map,
(c) Sample results in a frame of reference convecting at u(0,40) m/s, with identification of large-scale motion around x=1.5D.